CELL LINE

Establishment and characterization of a new intrahepatic cholangiocarcinoma cell line, ICC-X3

Hao Xu[1] · Wei Luo[1] · Zhenjie Zhao[1] · Xin Miao[2] · Changpeng Chai[1] · Jinjing Hu[1] · Huan Tang[3] · Hui Zhang[4] · Wence Zhou[3,4]

Abstract

Intrahepatic cholangiocarcinoma (ICC) is an aggressive cancer of the biliary tract that is prone to recurrence and metastasis and is characterized by poor sensitivity to chemotherapy and overall prognosis. To address this challenge, the establishment of suitable preclinical models is critical. In this study, we successfully established a new ICC cell line, named ICC-X3, from the satellite lesions of one ICC patient. The cell line was characterized with respect to phenotypic, molecular, biomarker, functional and histological properties. STR confirmed that ICC-X3 was highly consistent with primary tumor tissue. ICC-X3 cells positively expressed CK7, CK19, E-cadherin, vimentin, and Ki67. ICC-X3 was all resistant to gemcitabine, paclitaxel, 5-FU, and oxaliplatin. The cell line was able to rapidly form xenograft tumors which were highly similar to the primary tumor. The missense mutation of *TP53* exon was detected in ICC-X3 cells. ICC-X3 can be used as a good experimental model to study the progression, metastasis, and drug resistance of ICC.

Keywords Intrahepatic cholangiocarcinoma · Cell line · Establishment · Xenograft · Drug resistance

Hao Xu, Wei Luo, and Zhenjie Zhao contributed equally to this work and share first authorship.

✉ Hao Xu
amoyxu@126.com

✉ Hui Zhang
ery_huizhang@lzu.edu.cn

✉ Wence Zhou
zhouwc129@163.com

1 The Forth Department of General Surgery, the First Hospital of Lanzhou University, No. 1, Donggang West Road, LanZhou 730000, Gansu, China

2 State Key Laboratory of Veterinary Etiological Biology, Key Laboratory of Animal Virology of the Ministry of Agriculture, Lanzhou Veterinary Research Institute, Chinese Academy of Agricultural Sciences, LanZhou 730000, China

3 The Second Clinical Medical College, Lanzhou University, Lanzhou 730000, China

4 Department of General Surgery, the Second Hospital of Lanzhou University, Lanzhou 730000, China

Introduction

Intrahepatic cholangiocarcinoma (ICC) is a highly aggressive liver malignancy that originates from the intrahepatic bile ducts, and is the second most common primary liver cancer, accounting for 6.4–12% of all primary hepatic malignancies [1–3]. Although the incidence of ICC is relatively low, an upward trend has been observed over the past few decades [4, 5]. Due to the lack of pathognomonic signs and symptoms in the early stages and the absence of specific tumor markers, most ICC patients are already in the advanced stages of the disease at the time of diagnosis, and only 23–53% of patients have the opportunity for surgery [6, 7]. Unfortunately, a high recurrence rate after surgery also results in a poor disease prognosis. Even after radical resection, more than half of patients experience recurrence and eventually die [8–10]. Traditional chemotherapy with gemcitabine combined with platinum, as well as the use of targeted therapy and immunologic agents, are often the only options for patients with advanced disease stages, albeit with limited survival benefits. Since biliary tract tumors have high endogenous or acquired resistance to chemotherapy drugs, the therapeutic effect in patients is severely limited [11, 12].

Cell lines are in vitro models that are widely used in various fields of medical research, especially in basic tumor research and drug discovery. They provide unlimited quantities of homogeneous biomaterials for experimental purposes [13]. Each cell line has unique characteristics that reflect specific genotypes, sex-related properties, and patient-related phenotypes that make them of significant scientific and commercial value [14]. However, cell lines undergo phenotypic and genetic changes over long-term use. Other serious factors that greatly affect the results of subsequent experiments are cross-contamination or cell line misidentification during culture [15].

The etiology of ICC is diverse. The tumors are highly heterogeneous and ethnic factors also have a huge impact on drug efficacy. It is, therefore, important to use appropriate preclinical models that reflect these characteristics. So far, the established ICC cell lines still cannot meet these needs [16–19]. Hence, there is still an urgent need to continuously establish new ICC cell lines.

In this study, we successfully established a stable ICC cell line, named ICC-X3, using surgically resected satellite lesions from the ICC patient. The cell line can rapidly form xenograft tumors in nude mice and exhibit natural multidrug resistance to commonly used clinical chemotherapeutic agents. This newly established cell line provides a useful model for the study of ICC.

Materials and methods

Tissue source and ethics approval

This study was approved by the Medical Ethics Committee of the First Hospital of Lanzhou University (LDYYLL2022-345), and the patient signed the informed consent.

This patient was a 62-year-old female with a liver tumor and she received S4b hepatectomy in the First Hospital of Lanzhou University on July 23, 2021. The tissue sample was obtained from the surgically resected tumor. This patient did not receive systemic treatment before surgery. CT scan showing a large 9×7 cm lesion in segment IV of the liver (Fig. 1a). The primary tumor in the S4b segment of the liver was confirmed during the operation. There were multiple satellite lesions around the primary tumor (Fig. 1b).

Establishment of cell line

The freshly excised tumor tissue sample was immersed in sterile PBS (Gibco) 3–5 times, cut into small pieces of about 1 mm^3 and treated with type II collagenase (Gibco) and neutral protease (Invitrogen) at 37 °C for 1 h. The tissue blocks were agitated by pipette mixing every 15 min for about 1 min. The resulting supernatant was then collected and filtered using a 100-mesh filter, followed by centrifugation at 300xg for 3 min. The supernatant was discarded, then the residues were resuspended in PBS and centrifuged at 300xg for 3 min. The pellet was then resuspended with complete medium (RPMI-1640 supplemented with 10% FBS, 1% penicillin–streptomycin, Biological Industries), and was uniformly seeded in six-well plates (NEST). The mixed fibroblasts during the primary culture were mechanically scraped repeatedly with a pipette tip under the microscope to purify the epithelial cells. After about 2 weeks, upon reaching the full confluency, the culture medium was removed by suction, and the cells were rinsed twice with PBS and digested with 0.25% trypsin (Gibco) for passage. The growth of cells was periodically monitored under an inverted phase contrast microscope. From passage 4 onwards, cells were passaged at a 1:2 ratio and cryopreserved in serum-free Rapid Cell Freezing Buffer (Mei5 Biotechnology).

### Tumorsphere formation assays

ICC-X3 cells (p35) in the logarithmic growth phase were harvested, digested, centrifuged, washed twice with PBS, and placed in stem cell culture medium (RPMI-1640 supplemented with $1 \times$ B27, 20 ng/mL bFGF, and 20 ng/mL EGF). Cells were resuspended and counted. The cells were then seeded in ultra-low attachment cell culture 6-well plates (Corning) at a density of 1,000 cells/well, and 2 mL of culture medium was added daily for 14 days. Cultures were observed under a microscope to monitor the formation of spheroids.

Organoid culture

The matrigel (BD-Pharmingen) was placed at 4 °C to dissolve in advance. Meanwhile, the 24-well plates and centrifuge tubes were pre-cooled at -20 °C. ICC-X3 cells (p35) in the logarithmic growth phase were harvested, digested, resuspended, and counted. Then, 30 μL of matrigel and 30μL of organoid medium were added to 1×10^4 cells. All procedures were done on ice to prevent the formation of air bubbles. The 24-well plates were placed in a 37 °C incubator and incubated for 30 min. Upon solidification of the matrigel, 500 μL of the complete medium was added to each well to cover the droplets, and the cells were cultured in a 37 °C incubator. The complete medium was changed every 2 days. The morphological changes of the organoids were evaluated under a light microscope (Leica, S40-SLIder).

Cell growth curve

ICC-X3 cells (p30) in the logarithmic growth phase was harvested. The cell density was adjusted to 1×10^4 cells/mL
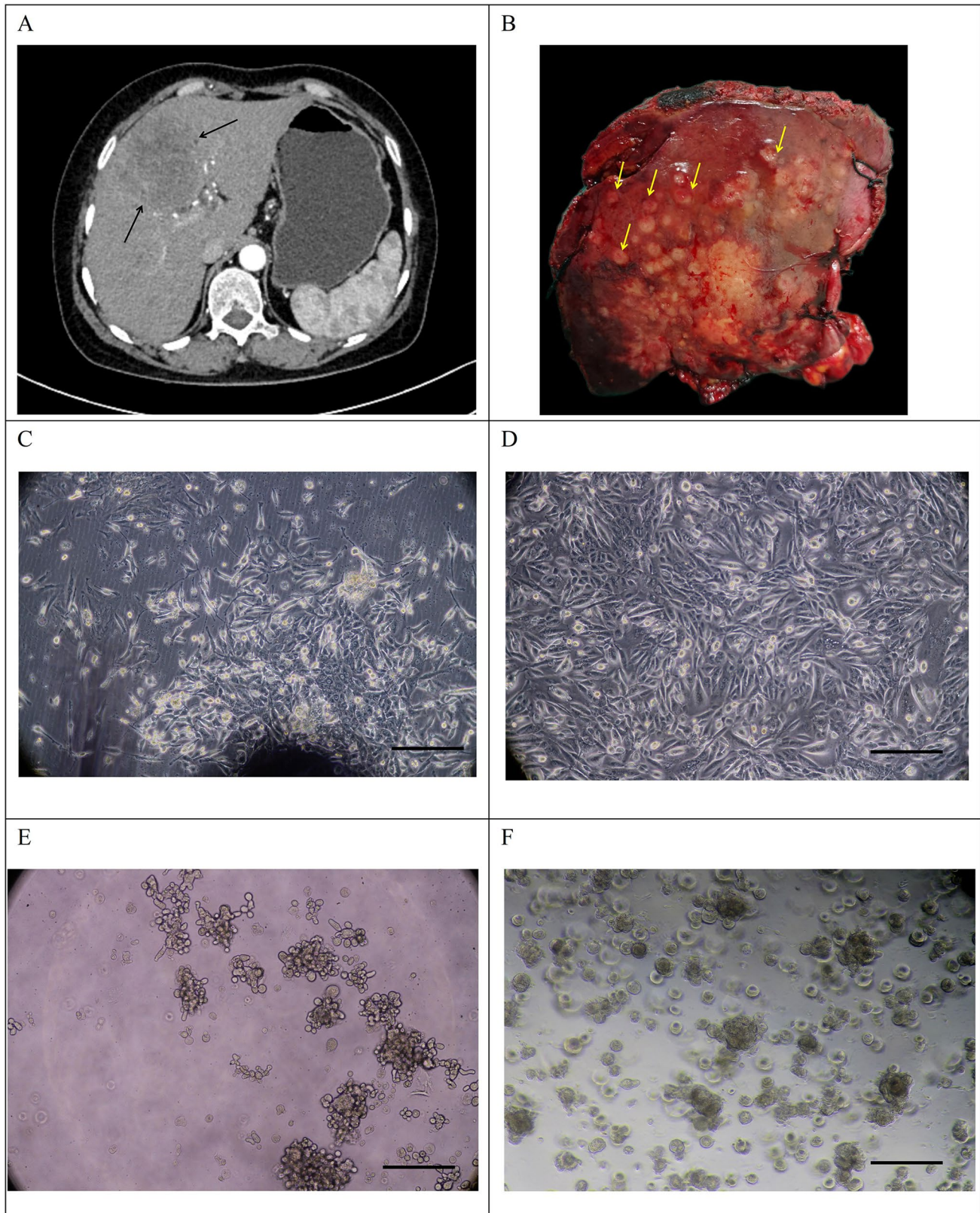
Fig. 1 Morphology, tumorsphere and organoid culture of ICC-X3 cells. **A** CT scan showing a large 9×7 cm lesion in segment IV of the liver (black arrows). **B** Gross view of the surgically resected specimen. Multiple satellite lesions can be seen around the primary lesion (yellow arrows). **C** shows an image of day 3 of the primary culture. **D** shows an image of thawed passage 90 of the ICC-X3 cells. **E** shows an image of tumorsphere culture of ICC-X3 cells. **F** shows an image of organoid culture of ICC-X3 cells. Scale bars, 100 μm

after trypsin digestion, and 0.1 mL per well of cell suspension was inoculated into a 96-well plate after mixing. Five duplicate holes were selected. After inoculation, the cells were treated with CCK-8 (Dojindo) reagent for 2 h at the same time, for 4 consecutive days, and the UV absorbance value at 450 nm was measured using a microplate reader (Biotek, synergy H1). The cell doubling time was calculated using the formula $Td = t \times lg2/lg(N1/N0)$. The cell growth curve was constructed with the time on the horizontal axis and the absorbance value on the vertical axis.

Short tandem repeat (STR) analysis

ICC-X3 cells (p15) in the logarithmic growth phase were collected by trypsinization. The sample, together with the primary tumor tissue, were sent to Genetic Testing Biotechnology Corporation (Suzhou, China) for STR analysis to check for cross-contamination during culture.

Karyotypic analysis

ICC-X3 cells (p35) in the logarithmic growth phase were treated with 0.25 µg/mL colchicine for 6 h and overnight at 37 °C. Metaphase cells were collected and fixed using a 3:1 methanol-glacial acetic acid solution. Samples were digested with trypsin, stained with Giemsa stain, and counted under a microscope. The well-dispersed, moderately stained split phase was selected for karyotype analysis.

Pharmaceutical agents

Gemcitabine was obtained from Jiangsu Hansoh Pharmaceutical Group Co., Ltd.

Oxaliplatin was obtained from Jiangsu Hengrui Pharmaceutical Co., Ltd. 5-FU was obtained from Tianjin Jinyao Pharmaceutical Co., Ltd. Paclitaxel was obtained from Jiangsu Osaikang Pharmaceutical Co., Ltd.

Drug sensitivity test

ICC-X3 cells (p50) were collected and prepared into a single-cell suspension after trypsinization. Then, cells were seeded in 96-well plates at a density of 100 cells/µL, and each group was repeated with 6 replicates. After the cells adhered, different concentrations of antitumor drugs were added to the experimental group, and equal volumes of solvent of each drug group were added to the vehicle control group. After 72 h of drug treatment, the spent media was replaced with complete media with 100 µL of serum-free medium containing 10% (v/v) CCK8. After 2 h of incubation, the OD value at 450 nm was measured.

BALB/c nude mice

The experimental animal models used in this study were all female BALB/c nude mice, 4–6 weeks old, weighing 16–20 g. The mice models were purchased from Changzhou Cavens Laboratory Animal Co., Ltd., and kept in the SPF laboratory of Lanzhou University Animal Experiment Center. All animal experiments were approved by the Ethics Committee of Medical Animal Experiments of the First Hospital of Lanzhou University (LDYYLL2022-345).

Xenograft formation assay

ICC-X3 cells (p40) in the logarithmic growth phase were harvested, and the cell density was adjusted to 1×10^7/mL after trypsinization. After mixing, 0.1 mL of each cell suspension was inoculated into the middle and posterior parts of the left armpit of BALB/c nude mice. The cell line was inoculated into 3 BALB/c nude mice, and the tumor growth in the nude mice was observed and recorded every other day. Tumor-bearing mice were sacrificed after 4 weeks of incubation. The tumor tissue was excised, fixed with 10% formalin, and subjected to routine histopathological and immunohistochemical (IHC) examinations.

Immunohistochemical staining

ICC-X3 cells (p40) in the logarithmic growth phase were seeded onto sterile glass slides after trypsinization. The glass slides were incubated for 48 h, then the slides were washed with PBS, fixed with 4% paraformaldehyde for 15 min, air-dried, and treated with 0.5% Triton X-100 for 20 min. Paraffin sections of the transplanted tumors and organoids were prepared and baked at 60 °C overnight. Deparaffinization, gradient alcohol hydration, and antigen retrieval were performed using the Autostainer Link 48 instrument (Dako). Then, the slides were incubated at 37 °C with 3% hydrogen peroxide solution for 15 min to block peroxidase activity. Next, 100 µL of normal goat serum was added dropwise and the tissue samples were blocked at 37 °C for 15 min. Primary antibodies (CK7, CK19, Ki67, E-cadherin, Vimentin, Fuzhou Maixin) were incubated at 37 °C for 1 h. The DAB staining solution kit (Dako) was used for color development and washed with running water for 5 min. After counterstaining with hematoxylin, the slides were then sealed with neutral resin and observed under a light microscope (Olympus, IX73 + DP74).

TP53 mutation screening

The coding region mutations of *TP53* was evaluated in ICC-X3 (p45) cells. Total mRNA was extracted. After genomic DNA was removed, we conducted reverse transcription

Table 1 Primer sequences for the amplification of *TP53* exons

Primer name	Sequences
TP53-F	ATGGAGGAGCCGCAGTCAG
TP53-R	TCAGTCTGAGTCAGGCCC

to synthesize cDNA. Finally, we used cDNA as template, upstream primer TP53-F: ATGGAGGAGCCGCAGTCAG, and downstream primer TP53-R: TCAGTCTGAGTCAGG CCC to conduct PCR (Table 1). The PCR product was connected to the T plasmid and then coated. The PCR products were purified using the Shanghai Sangon PCR product purification kit and were sent to Shanghai Sangon Company for sequencing. The sequencing results of the amplified fragments were aligned with the reference sequence using NCBI.

Statistical analyses

All statistical analyses were performed using the SPSS 22.0 software. The data were expressed as mean $\pm$ SD. Student's *t* tests and ANOVA were used for group comparisons. A *P* value of < 0.05 was considered statistically significant.

Results

Establishment of cell line

The satellite lesions were obtained aseptically, followed by enzymatic digestion for primary culture and subculture. The fibroblasts were then removed by mechanical scraping to establish a stable passage of human ICC cell line, named ICC-X3. The cells have been stably passaged for more than 90 generations and have been deposited in the China Center for Type Culture Collection (CCTCC NO: 202260). Observed under a light microscope, the cell line grew adherently and lost contact inhibition. The cells exhibited a spindle-shaped morphology, with a small amount of polygonal and round cells (Fig. 1c). The nucleus is obvious, the cells of each generation always maintain vigorous metabolism, the cell shape is stable even if it was already passed to the 90th generation, and the cell shape and growth rate remain unchanged (Fig. 1d).

Tumorsphere and organoid culture

Under serum-free conditions, ICC-X3 cells were able to grow in suspension and formed well-structured cholangiocarcinoma spheres in ultra-low attachment plates, indicating that ICC-X3 may have stem cell properties (Fig. 1e).

When ICC-X3 cells were inoculated into matrigel, the formed organoids gradually increased from small granules to single spheroids or spore-like aggregates of multiple spheroids with different sizes. This culturing process took 7 to 14 days, depending on the characteristics of the cell itself (Fig. 1f).

DNA STR analysis

The DNA typing results indicated that the two submitted samples were from the same individual with a likelihood ratio (LR) of 5.0731×10^{20}. It suggests that ICC-X3 cells are highly consistent with the STR analysis of the primary tissue source (Fig. 2a).

Cell growth curve

The cell proliferation was observed by measuring the absorbance value of cells at 450 nm using a CCK-8 assay for 4 consecutive days. The cell growth curve was constructed with the culture time as the abscissa and the absorbance value as the ordinate. According to the formula: $Td = t lg2/lg(N1/N0)$, the doubling time of ICC-X3 cells was 36 h (Fig. 2b).

Karyotypic analysis

Ten well-dispersed and moderately stained split phases were selected for chromosome counting and analysis. The results showed that ICC-X3 exhibited hypotetraploid karyotypes with large differences in chromosome number and morphology. The representative karyotype of ICC-X3 is 81,XXX del(6) (p21),

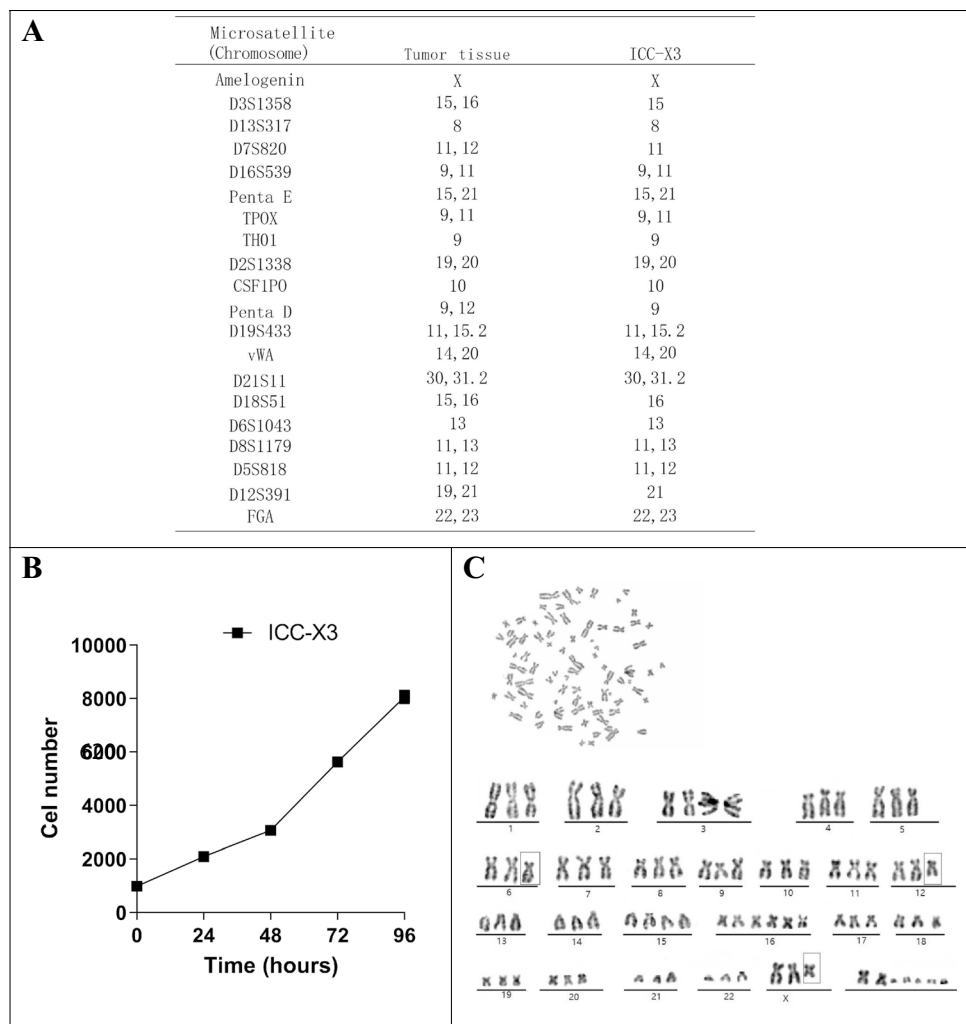del(12)(q23), del(X)(q13), $+3, +15, +16(\times 3), + mar(\times 7)$ (Fig. 2c).

Drug sensitivity test

Oxaliplatin, 5-FU, paclitaxel and gemcitabine are the most commonly used chemotherapeutic drugs for bile duct malignancies. We evaluated the susceptibility of ICC-X3 to oxaliplatin, 5-FU, paclitaxel and gemcitabine (the IC50 values being 38.36 µM, 119.5 µM, 11.21 ng/ml and 18.18 µM, respectively) and the results showed that ICC-X3 cells exhibited natural resistance to all four chemotherapeutic drugs (Fig. 3a–d).

Xenograft formation assay

ICC-X3 cell suspensions were subcutaneously inoculated into 3 BALB/c nude mice and showed 100% tumorigenicity (Fig. 4a). The xenograft tumors grew rapidly, infiltrating growth to surrounding tissues (Fig. 4b). The diameter of the tumor was close to 1 cm at 4 weeks (Fig. 4c). In the transplanted mice, no metastatic lesions were found in other organs within 4 weeks (Fig. 4d). Figure 4e,and 4f shows the tumor volume and weight curve of BALB/c nude mice.

Fig. 2 STR analysis, cell growth curve and karyotypic analysis of ICC-X3 cells. **A** The STR analysis shows that ICC-X3 cells are highly consistent with the primary tumor. **B** The growth curve of ICC-X3 cells. The doubling time of ICC-X3 cells was 36 h. **C** The cells exhibited hypotetraploid karyotypes with large differences in chromosome number and morphology. The representative karyotype of the ICC-X3 cells was 81,XXX del(6) (p21), del(12)(q23), del(X)(q13),+3,+15,+16(×3) ,+mar(×7)

Microsatellite (Chromosome)	Tumor tissue	ICC-X3
Amelogenin	X	X
D3S1358	15, 16	15
D13S317	8	8
D7S820	11, 12	11
D16S539	9, 11	9, 11
Penta E	15, 21	15, 21
TPOX	9, 11	9, 11
TH01	9	9
D2S1338	19, 20	19, 20
CSF1PO	10	10
Penta D	9, 12	9
D19S433	11, 15. 2	11, 15. 2
vWA	14, 20	14, 20
D21S11	30, 31. 2	30, 31. 2
D18S51	15, 16	16
D6S1043	13	13
D8S1179	11, 13	11, 13
D5S818	11, 12	11, 12
D12S391	19, 21	21
FGA	22, 23	22, 23

HE and immunohistochemical staining

HE staining showed that ICC-X3 cells exhibited a spindle-shaped morphology, with enlarged nuclei, obvious nucleoli, and less cytoplasm (Fig. 5a). HE staining of organoids showed that ICC-X3 formed gland-like structures. The cells in the spheroid are closely connected, and there are lumen-like structures inside. The contents of the cavity have no cellular components (Fig. 5b).

The postoperative pathological diagnosis of the primary tumor showed moderately to poorly differentiated ICC (Fig. 5c1), some of which are undifferentiated carcinoma (Fig. 5c2).

HE staining of the xenograft tumor showed that the nuclei of the transplanted tumor was deeply stained, the nucleoli were obvious, the cytoplasmic foam was transparent, and there were a lot of mitotic figures. The cell morphology in the xenograft tumor was different. Some cells formed gland-like structures (Fig. 5d1), while some cells were spindle-shaped (Fig. 5d2), similar to fibroblasts. These indicated that ICC-X3 cells retained good tumor heterogeneity of the primary tumor.

Further IHC detection of cell lines, organoids, and transplanted tumor showed positive expression of CK7 (Fig. 6a1–c1) and CK19 (Fig. 6a2–c2), confirming that they originated from bile duct epithelium. Ki67 was expressed in a high proportion among them, which is consistent with the rapid tumor proliferation and illustrates the malignant characteristics of the tumors (Fig. 6a3–c3). The simultaneous expression of E-cadherin (Fig. 6a4–c4) and vimentin (Fig. 6a5–c5) indicates that these cells have EMT characteristics, which is also consistent with the clinical manifestations of multiple satellite lesions.

TP53 mutation screening

PCR gel electrophoresis showed that the full-length fragment of *TP53* was successfully cloned (Fig. 7a). By designing primer PCR and sequencing, it is found that the *TP53* gene of most cells in ICC-X3 has C mutation to T (Fig. 7b),

Fig. 3 Drug sensitivity of ICC-X3 cells. Figures showing the dose-dependent effect of oxaliplatin (**A**), 5-FU (**B**), paclitaxel (**C**) and gemcitabine (**D**) in ICC-X3 cells. The cell line exhibited natural resistance to the four chemotherapeutic drugs
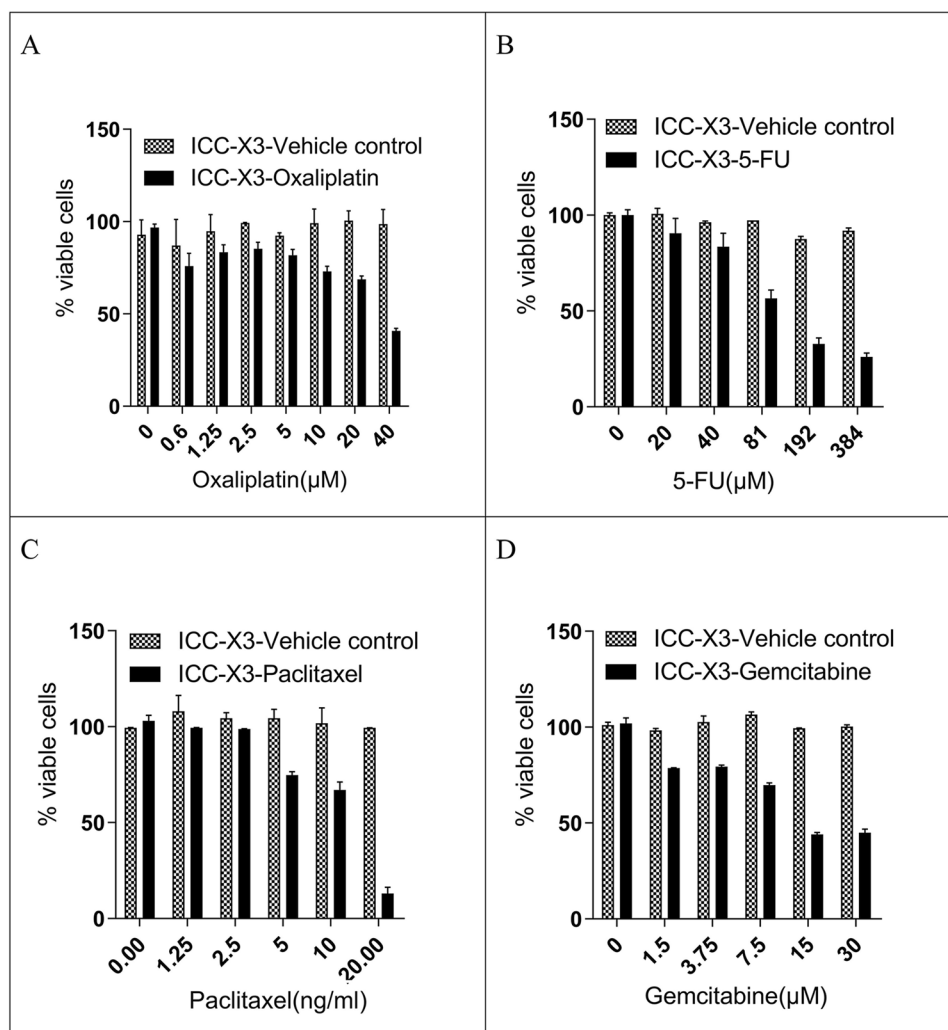
and Fig. 7c is the antisense chain of the reference sequence, so it shows that G mutation to A.

Discussion

ICC is a highly lethal disease with a poor prognosis. Postoperative recurrence and drug resistance are the main causes of death in patients [1–3]. There are only a few reports on the establishment of ICC cell lines; however, to account for the high heterogeneity of ICC and the influence of ethnic differences, it is necessary to continuously establish new ICC cell lines for further research. Unfortunately, in recent years, the incidence of this disease has gradually increased in China, but compared with Japan and South Korea, there are few reports on the establishment of Chinese-derived ICC cell lines [20–22]. This is incompatible with China's huge population. To further study the characteristics of ICC in the Chinese population, more Chinese-derived ICC cell lines need to be established.

In this study, a new ICC cell line, ICC-X3, was established by primary culture and subculture after enzymatic digestion. The cell line proliferates vigorously and can provide a sustainable in vitro model for basic and clinical studies on ICC. HE staining of ICC-X3 showed that the cells were morphologically diverse, mainly spindle-shaped, with enlarged nuclei, deepened staining, and an imbalanced ratio of nucleus to the cytoplasm, similar to HuH-28 cells [23]. IHC staining showed that ICC-X3, as well as its corresponding organoids and transplanted tumors, positively expressed CK7, CK19, E-cadherin, vimentin, and Ki67. These indicating the retention of most of the genetic properties of the primary tumor.

ICC-X3 displayed a strong tumor spheroid formation ability in ultra-low attachment plates and was able to form organoids in matrigel. These data indicate that it has strong stem cell properties [24].

Previous studies have found that the more aggressive cells form branched organoids, and the less aggressive cell lines mostly form spherical organoids. The ICC-X3 cell line
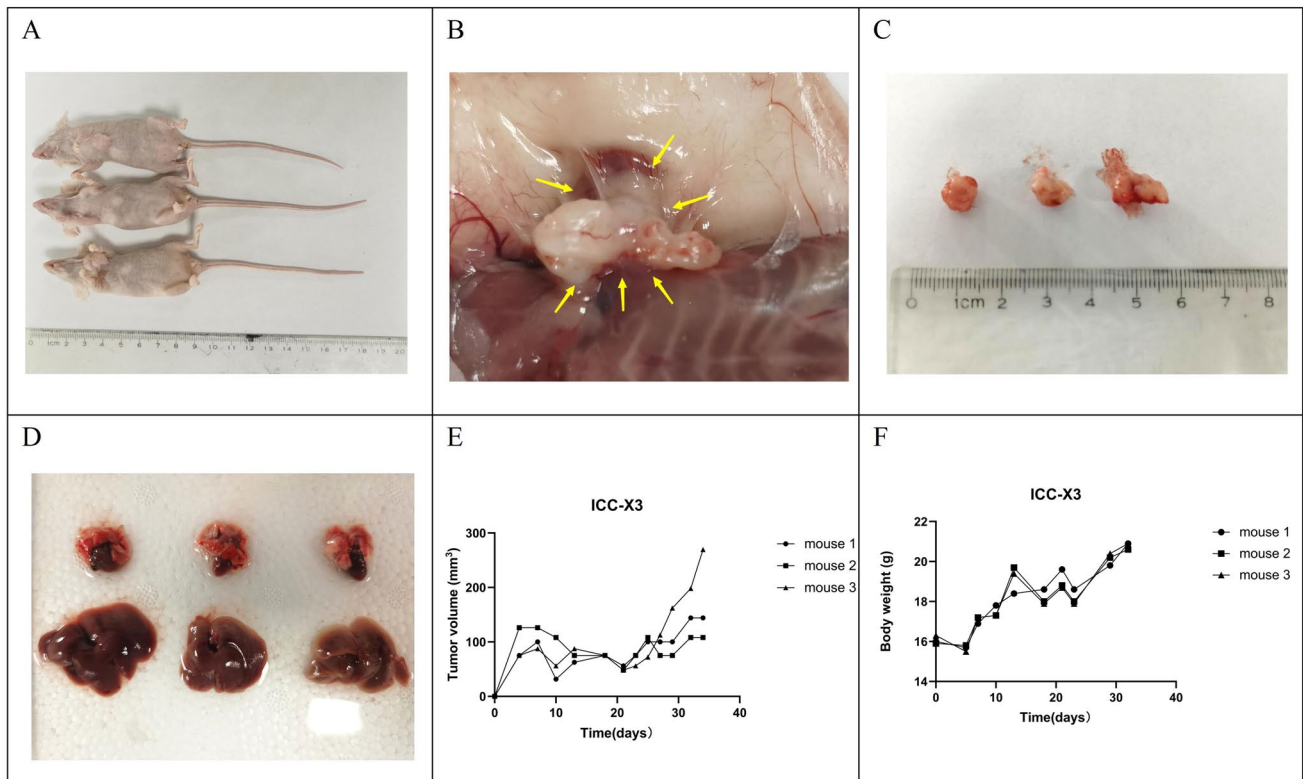
Fig. 4 Tumorigenicity in BALB/C nude mice. **A** ICC-X3 rapidly formed xenografts after inoculation into the BALB/C nude mice and showed 100% tumorigenicity. **B** The xenograft tumors grew rapidly, infiltrating growth to surrounding tissues (yellow arrow). **C** The diameter of the tumor was close to 1 cm at 4 weeks. **D** No metastatic lesions were found in the lung and liver tissues of the BALB/C nude mice. **E** shows the tumor volume curve of BALB/c nude mice. **F** shows the weight curve of BALB/c nude mice

in this study was from moderately to poorly differentiated ICC tissues, and some were derived from undifferentiated carcinomas. The formed tumor spheres and organoids were branched, similar to those reported in the literature [25].

Chromosomal instability is closely related to tumorigenesis. Chromosomal instability is not necessarily the direct cause of cell carcinogenesis, but genetic instability may lead to the activation of oncogenes in cells or the inactivation or deletion of anti-cancer genes, which in turn induces cell carcinogenesis [26–28]. In this study, our karyotype analysis showed that ICC-X3 was hypotetraploid, which was different from 82.3, HKGZ-CC, MT-CHC01, and other karyotypes, which fully reflected the great chromosomal differences between tumors. It can be used as a useful model for an in-depth study of the mechanism of chromosomal abnormalities in tumors [20, 29, 30].

Chemotherapy is one of the main components of comprehensive treatment for patients with advanced ICC. However, due to the different hereditary patterns of drug-metabolizing enzymes in patients and the heterogeneity of tumors, the sensitivity of individual patients to different chemotherapeutic drugs is different, with even the possibility of congenital resistance [31]. In this study, ICC-X3 was naturally resistant to gemcitabine, paclitaxel, 5-FU, and oxaliplatin, similar to 82.3. This indicates that ICC-X3 is a multi-drug-resistant cell line, which is a good model for drug resistance mechanism studies.

Human cell line-derived xenograft tumor models (CDX) are widely used in the study of the in vivo biological behavior of tumors, preclinical testing of pharmacodynamics, and the development of new antitumor drugs [32]. However, not all tumor cell lines, such as TKKK, HuH-28, RBE, HCCC-9810, etc., can form xenografts after inoculation into immunodeficient mice, which greatly limits tumor biology research and new drug development [23, 33]. In this study, ICC-X3 cell line was able to rapidly form xenografts in immunodeficient mice, with a short incubation period and a 100% xenograft formation rate. Moreover, cell suspension in matrigel and additional growth factors before inoculation are not needed, showing that the inoculation process is simple and convenient.

It has been found that 37% of ICCs have mutations in the *TP53* gene [34]. Mutations in the *TP53* gene not only lead to the loss of its tumor suppressor function but also promotes the occurrence and development of tumors, a phenomenon known as gain-of-function (GOF)
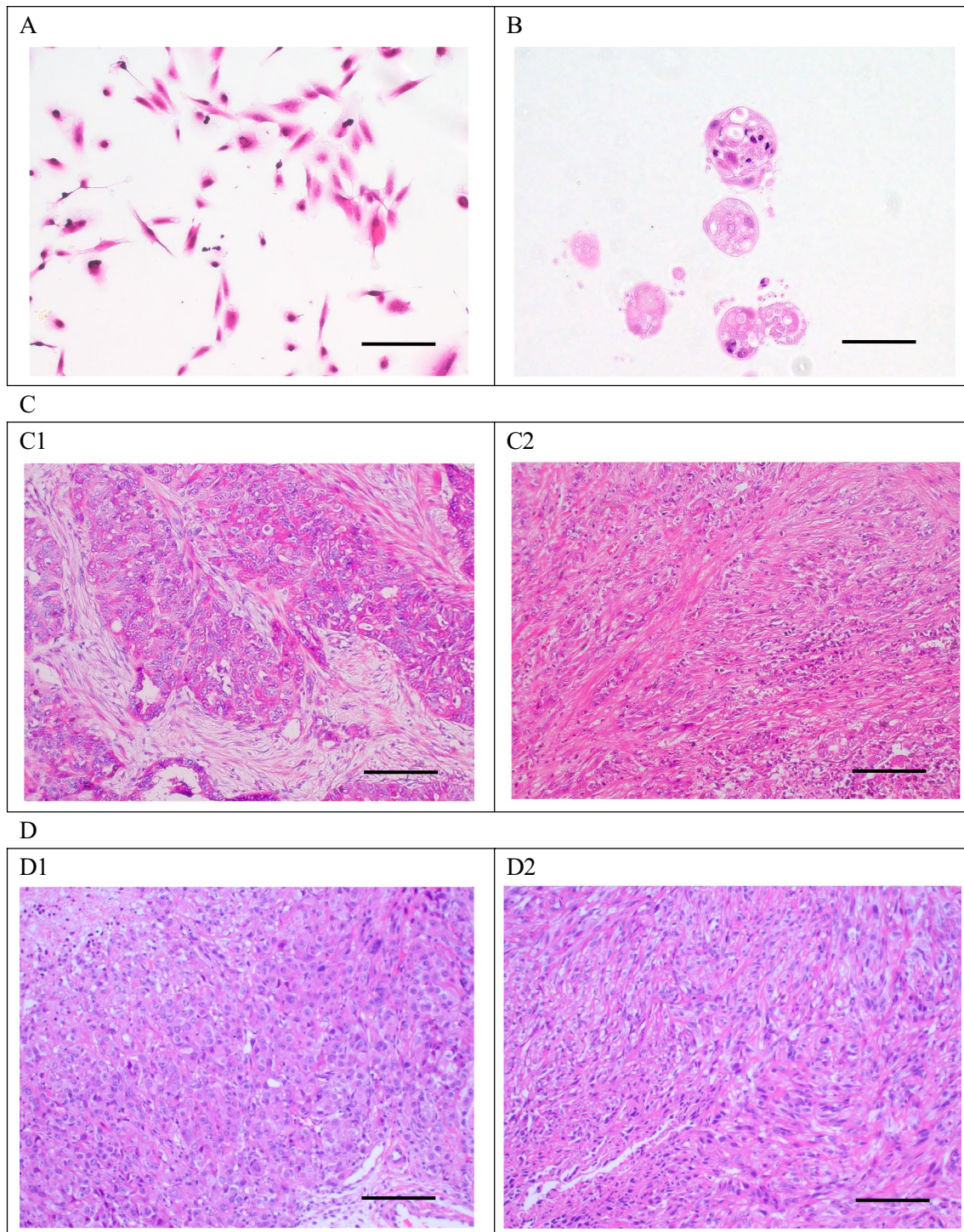
Fig. 5 HE staining of ICC-X3 cells, organoids, primary tumor and xenograft tumor. **A** HE staining showed that ICC-X3 cells exhibited a spindle-shaped morphology, with enlarged nuclei, obvious nucleoli, and less cytoplasm. **B** HE staining of organoids showed that ICC-X3 formed gland-like structures. The cells in the spheroid are closely connected, and there are lumen-like structures inside. The contents of the cavity have no cellular components. **C** HE staining of the primary tumor showed that it was moderately to poorly differentiated ICC (**C1**), some of which are undifferentiated carcinoma (**C2**). **D** HE staining of the xenograft tumor showed that the nuclei of the xenograft tumor was deeply stained, the nucleoli were obvious, the cytoplasmic foam was transparent, and there were a lot of mitotic figures. The cell morphology in the xenograft tumor was different. Some cells formed gland-like structures (**D1**), while some cells were spindle-shaped (**D2**), similar to fibroblasts. Scale bars, 100 µm
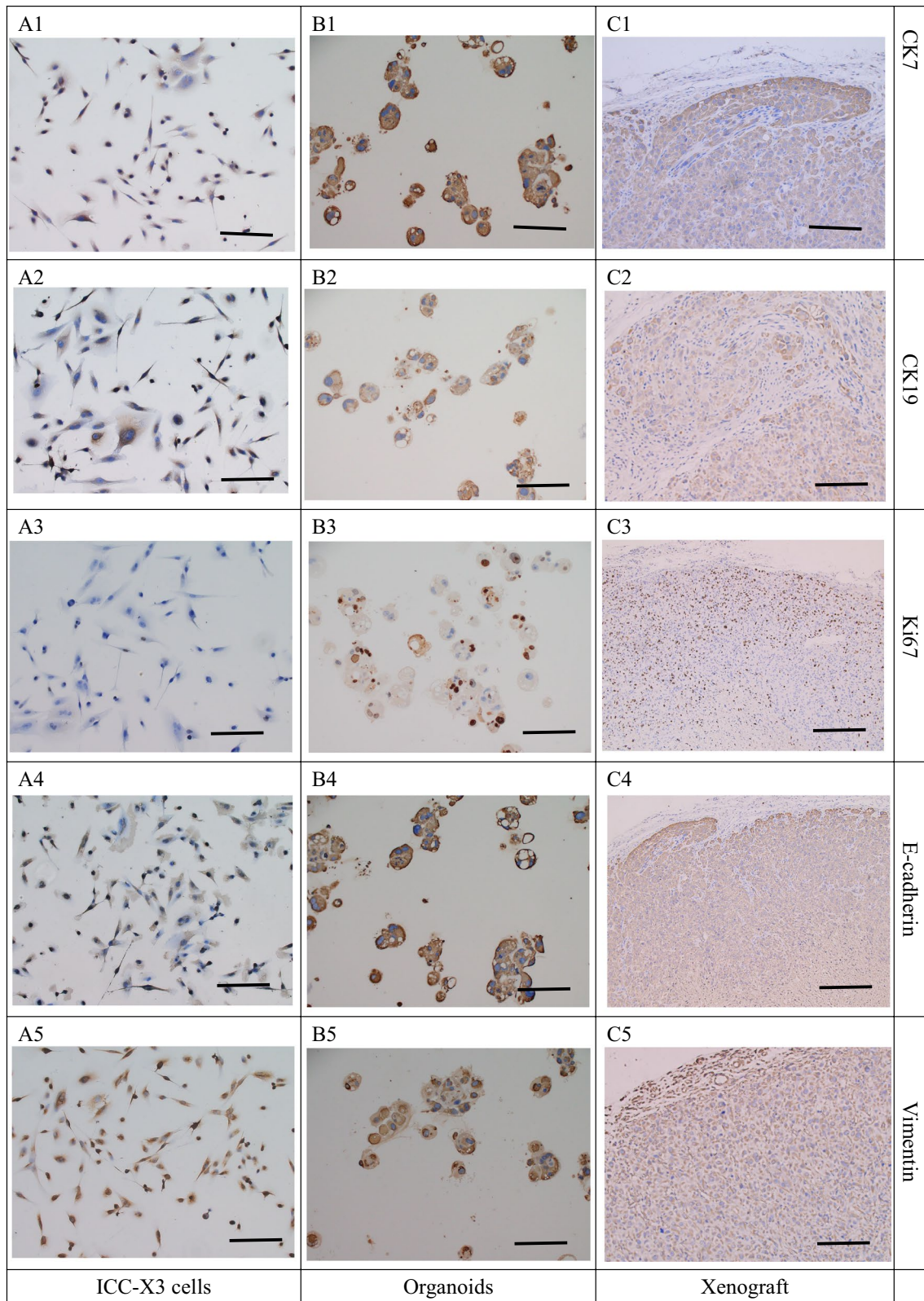
Fig. 6 Immunohistochemical staining of ICC-X3 cells, organoids and xenograft tumor. CK7 positive staining in ICC-X3 cells (**A1**), organoids (**B1**), xenograft tumor (**C1**). CK19 positive staining in ICC-X3 cells (**A2**), organoids (**B2**), xenograft tumor (**C2**). Ki-67 positive staining in ICC-X3 cells (**A3**), organoids (**B3**), xenograft tumor (**C3**). E-cadherin positive staining in ICC-X3 cells (**A4**), organoids (**B4**), xenograft tumor (**C4**). Vimentin positive staining in ICC-X3 cells (**A5**), organoids (**B5**), xenograft tumor (**C5**). Scale bars, 100 μm
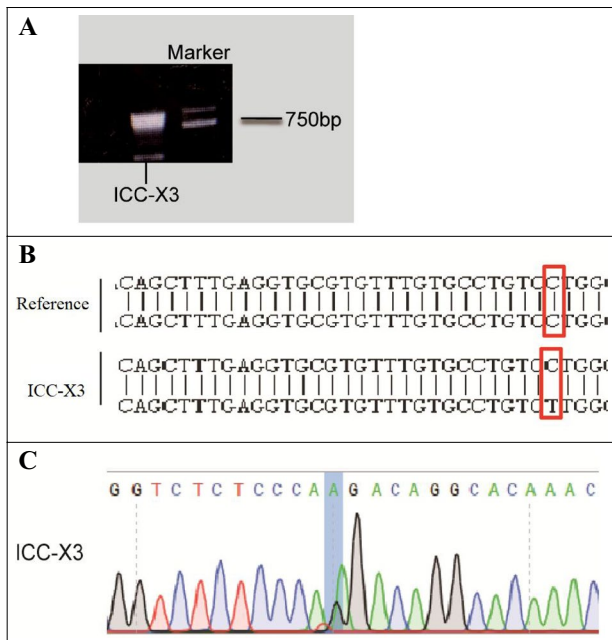
Fig. 7 *TP53* mutation detection. **A** PCR gel electrophoresis showed that the full-length fragment of TP53 was successfully cloned. **B** By designing primer PCR and sequencing, it was found that the TP53 gene of most cells in ICC-X3 has C mutation to T. **C** The antisense chain of the reference sequence showed that G mutation to A

[35]. About 80% of *TP53* mutations are single-site point mutations. Mutations in *TP53* are associated with tumor progression, metastasis, recurrence, and drug resistance, and *TP53* expression tends to increase with tumor aggressiveness [36–39]. Previous studies demonstrate that *TP53* mutation frequency is about 10% in primary prostate cancer but up to 50% in metastases, which is associated with poor overall survival and progression-free survival [40]. In this study, a missense mutation in *TP53* was found in the ICC-X3 cell line, the mutated protein was related to the enhanced ability of cell invasion and metastasis.

In conclusion, a new ICC cell line was established from the metastatic lesions. The cell line can be used as a good cellular model to study the biological behavior of ICC and develop new therapeutic strategies.

Declarations

Conflict of interest The authors declare no competing interests.

Ethical approval The study was conducted according to the guidelines of the Declaration of Helsinki, and approved by the Ethics Committee of the First Hospital of Lanzhou University (LDYYLL2022-345).

Consent for publication We have obtained consents to publish this paper from all the participants of this study.

References

1. Alvaro D, Crocetti E, Ferretti S, Bragazzi MC, Capocaccia R, AISF Cholangiocarcinoma committee. Descriptive epidemiology of cholangiocarcinoma in Italy. Dig Liver Dis. 2010;42(7):490–5.
2. Kudo M, Izumi N, Kokudo N, Sakamoto M, Shiina S, Takayama T, et al. Report of the 22nd nationwide follow-up survey of primary liver cancer in Japan (2012–2013). Hepatol Res. 2022;52(1):5–66.
3. Petrick JL, Campbell PT, Koshiol J, Thistle JE, Andreotti G, Beane-Freeman LE, et al. Tobacco, alcohol use and risk of hepatocellular carcinoma and intrahepatic cholangiocarcinoma: the liver cancer pooling project. Br J Cancer. 2018;118(7):1005–12.
4. Shaib YH, Davila JA, McGlynn K, El-Serag HB. Rising incidence of intrahepatic cholangiocarcinoma in the United States: a true increase? J Hepatol. 2004;40(3):472–7.
5. Witjes CD, Karim-Kos HE, Visser O, de Vries E, IJzermans JN, de Man RA, et al. Intrahepatic cholangiocarcinoma in a low endemic area: rising incidence and improved survival. HPB. 2012;14(11):777–81.
6. Sakamoto Y, Kokudo N, Matsuyama Y, Sakamoto M, Izumi N, Kadoya M, Liver Cancer Study Group of Japan, et al. Proposal of a new staging system for intrahepatic cholangiocarcinoma: analysis of surgical patients from a nationwide survey of the liver cancer study group of Japan. Cancer. 2016;122(1):61–70.
7. Dover LL, Jacob R, Wang TN, Richardson JH, Redden DT, Li P, et al. Improved postoperative survival for intraductal-growth subtype of intrahepatic cholangiocarcinoma. Am Surg. 2016;82(11):1133–9.
8. Zhang XF, Beal EW, Bagante F, Chakedis J, Weiss M, Popescu I, et al. Early versus late recurrence of intrahepatic cholangiocarcinoma after resection with curative intent. Br J Surg. 2018;105(7):848–56.
9. Merath K, Mehta R, Hyer JM, Bagante F, Sahara K, Alexandrescu S, et al. Impact of body mass index on tumor recurrence among patients undergoing curative-intent resection of intrahepatic

cholangiocarcinoma- a multi-institutional international analysis. Eur J Surg Oncol. 2019;45(6):1084–91.

10. Hu LS, Zhang XF, Weiss M, Popescu I, Marques HP, Aldrighetti L, et al. Recurrence patterns and timing courses following curative-intent resection for intrahepatic cholangiocarcinoma. Ann Surg Oncol. 2019;26(8):2549–57.

11. Valle JW, Furuse J, Jitlal M, Beare S, Mizuno N, Wasan H, et al. Cisplatin and gemcitabine for advanced biliary tract cancer: a meta-analysis of two randomised trials. Ann Oncol. 2014;25(2):391–8.

12. Rueff J, Rodrigues AS. Cancer drug resistance: a brief overview from a genetic viewpoint. Methods Mol Biol. 2016;1395:1–18.

13. Mirabelli P, Coppola L, Salvatore M. Cancer cell lines are useful model systems for medical research. Cancers (Basel). 2019;11(8):1098.

14. Isidan A, Yenigun A, Soma D, Aksu E, Lopez K, Park Y, et al. Development and characterization of human primary cholangiocarcinoma cell lines. Am J Pathol. 2022;192(9):1200–17.

15. Fusenig NE, Capes-Davis A, Bianchini F, Sundell S, Lichter P. The need for a worldwide consensus for cell line authentication: experience implementing a mandatory requirement at the international journal of cancer. PLoS Biol. 2017;15(4): e2001438.

16. Komuta M. Intrahepatic cholangiocarcinoma: tumour heterogeneity and its clinical relevance. Clin Mol Hepatol. 2022;28(3):396–407.

17. Wang J, Sun Y, Bertagnolli MM. Comparison of gastric cancer survival between Caucasian and Asian patients treated in the United States: results from the surveillance epidemiology and end results (SEER) database. Ann Surg Oncol. 2015;22:2965–71.

18. Lin SJ, Gagnon-Bartsch JA, Tan IB, Earle S, Ruff L, Pettinger K, et al. Signatures of tumour immunity distinguish Asian and non-Asian gastric adenocarcinomas. Gut. 2015;64(11):1721–31.

19. Shi Y, Au JS, Thongprasert S, Srinivasan S, Tsai CM, Khoa MT, et al. A prospective, molecular epidemiology study of EGFR mutations in Asian patients with advanced non-small-cell lung cancer of adenocarcinoma histology (PIONEER). J Thorac Oncol. 2014;9(2):154–62.

20. Ma S, Hu L, Huang XH, Cao LQ, Chan KW, Wang Q, et al. Establishment and characterization of a human cholangiocarcinoma cell line. Oncol Rep. 2007;18(5):1195–200.

21. Guo SS, Wang Y, Fan QX. Raddeanin A promotes apoptosis and ameliorates 5-fluorouracil resistance in cholangiocarcinoma cells. World J Gastroenterol. 2019;25(26):3380–91.

22. Chen S, Chen Z, Li Z, Li S, Wen Z, Cao L, et al. Tumor-associated macrophages promote cholangiocarcinoma progression via exosomal Circ_0020256. Cell Death Dis. 2022;13(1):94.

23. Kusaka Y, Tokiwa T, Sato J. Establishment and characterization of a cell line from a human cholangiocellular carcinoma. Res Exp Med (Berl). 1988;188(5):367–75.

24. Eguchi T, Sheta M, Fujii M, Calderwood SK. Cancer extracellular vesicles, tumoroid models, and tumor microenvironment. Semin Cancer Biol. 2022. https://doi.org/10.1016/j.semcancer.2022.01.003.

25. Koike N, Todoroki T, Kawamoto T, Yoshida S, Kashiwagi H, Fukao K, et al. The invasion potentials of human biliary tract carcinoma cell lines: correlation between invasiveness and morphologic characteristics. Int J Oncol. 1998;13(6):1269–74.

26. Gemble S, Wardenaar R, Keuper K, Srivastava N, Nano M, Macé AS, et al. Genetic instability from a single S phase after whole-genome duplication. Nature. 2022;604(7904):146–51.

27. López S, Lim EL, Horswell S, Haase K, Huebner A, Dietzen M, et al. Interplay between whole-genome doubling and the accumulation of deleterious alterations in cancer evolution. Nat Genet. 2020;52(3):283–93.

28. Bielski CM, Zehir A, Penson AV, Donoghue MTA, Chatila W, Armenia J, et al. Genome doubling shapes the evolution and prognosis of advanced cancers. Nat Genet. 2018;50(8):1189–95.

29. Peraldo-Neia C, Massa A, Vita F, Basiricò M, Raggi C, Bernabei P, et al. A novel multidrug-resistant cell line from an Italian intrahepatic cholangiocarcinoma patient. Cancers (Basel). 2021;13(9):2051.

30. Cavalloni G, Peraldo-Neia C, Varamo C, Casorzo L, Dell'Aglio C, Bernabei P, et al. Establishment and characterization of a human intrahepatic cholangiocarcinoma cell line derived from an Italian patient. Tumour Biol. 2016;37(3):4041–52.

31. Dagogo-Jack I, Shaw AT. Tumour heterogeneity and resistance to cancer therapies. Nat Rev Clin Oncol. 2018;15(2):81–94.

32. Broutier L, Mastrogiovanni G, Verstegen MM, Francies HE, Gavarró LM, Bradshaw CR, et al. Human primary liver cancer-derived organoid cultures for disease modeling and drug screening. Nat Med. 2017;23(12):1424–35.

33. Enjoji M, Sakai H, Nawata H, Kajiyama K, Tsuneyoshi M. Sarcomatous and adenocarcinoma cell lines from the same nodule of cholangiocarcinoma. In Vitro Cell Dev Biol Anim. 1997;33(9):681–3.

34. Tannapfel A, Weinans L, Geissler F, Schütz A, Katalinic A, Köckerling F, et al. Mutations of p53 tumor suppressor gene, apoptosis, and proliferation in intrahepatic cholangiocellular carcinoma of the liver. Dig Dis Sci. 2000;45(2):317–24.

35. Yue X, Zhao Y, Xu Y, Zheng M, Feng Z, Hu W. Mutant p53 in cancer: accumulation, gain-of-function, and therapy. J Mol Biol. 2017;429(11):1595–606.

36. Sato Y, Harada K, Sasaki M, Nakanuma Y. Histological characterization of biliary intraepithelial neoplasia with respect to pancreatic intraepithelial neoplasia. Int J Hepatol. 2014;2014: 678260.

37. Moschovis D, Bamias G, Delladetsima I. Mucins in neoplasms of pancreas, ampulla of Vater and biliary system. World J Gastrointest Oncol. 2016;8(10):725–34.

38. Kozyrska K, Pilia G, Vishwakarma M, Wagstaff L, Goschorska M, Cirillo S, et al. p53 directs leader cell behavior, migration, and clearance during epithelial repair. Science. 2022;375(6581):eabl8876.

39. Qi LN, Ma L, Wu FX, Chen YY, Xu JX, Peng YC, et al. Clinical implications and biological features of a novel postoperative recurrent HCC classification: a multi-centre study. Liver Int. 2022;42(10):2283–98.

40. Zhang W, Dong Y, Sartor O, Zhang K. Deciphering the increased prevalence of TP53 mutations in metastatic prostate cancer. Cancer Inform. 2022;21:11769351221087046.